

Entropy driven thermo-gelling vitrimer

Xiuyang Xia,^{1,2,*} Peilin Rao,^{1,*} Juan Yang,³ Massimo Pica Ciamarra,² and Ran Ni^{1,†}

¹Chemical Engineering, School of Chemical and Biomedical Engineering,
Nanyang Technological University, 62 Nanyang Drive, Singapore 637459

²Division of Physics and Applied Physics, School of Physical and Mathematical Sciences,
Nanyang Technological University, 21 Nanyang Link, Singapore 637371

³Department of Chemistry, National University of Singapore, 117546 Singapore

Thermo-gelling polymers have been envisioned as promising smart biomaterials but limited to their weak mechanical and thermodynamic stabilities. Here we propose a new thermo-gelling vitrimer, which remains at a liquid state because of the addition of protector molecules preventing the crosslinking, and with increasing temperature, an entropy driven crosslinking occurs to induce the sol-gel transition. Moreover, we find that the activation barrier in the metathesis reaction of vitrimers plays an important role, and experimentally one can use catalysts to tune the activation barrier to drive the vitrimer to form an equilibrium gel at high temperature, which is not subject to any thermodynamic instability. We formulate a mean field theory to describe the entropy driven crosslinking of the vitrimer, which agrees quantitatively with computer simulations, and paves the way for design and fabrication of novel vitrimers for biomedical applications.

Thermo-gels are the polymer that undergoes a sol-gel transition with increasing temperature. Over the past decades, thermo-gels have gained extensive attention in biomaterials and biomedical sciences [1–4], because of their significant potentials in applications of shape-memory polymer [5], drug delivery [6–8], tissue engineering [9], bioseparations [10, 11], etc. The typical mechanism of thermo-gelling involves non-covalent interactions in the material such as hydrogen bonding [12], Coulombic [13], and competing van der Waals interactions [14]. By increasing temperature, the intra- and intermolecular interactions outbalance the solvent effect, and thereby results in the gelation of the material [15–17]. However, the weak non-covalent interaction usually leads to low mechanical stability and rapid disintegrations in physiological environments [18, 19]. To overcome those challenges, one may obtain a permanently crosslinked gelling networks with higher mechanical stability by using chemical reactions such as Michael addition [20], enzymatic crosslinking [21, 22], or photo-induced crosslinking [18, 23]. However, the gel formation requires an extra re-processing step that is difficult to control or not applicable for thick or opaque samples [24–26], and the formed gel would lose the reversibility.

Vitrimers are a unique type of crosslinked polymer networks with dynamic and exchangeable covalent bonds [27]. They have shown great promises as recyclable materials in chemical and materials industries. The exchangeability originates from the reversible reactions between polymer backbones and small crosslinkers through metathesis reactions. The rate of these reactions is governed by temperature, and some of them, e.g., silyl ether metathesis [28], thio-disulfide exchange reaction [29, 30], dynamic Schiff base [31, 32], are biocompatible and applicable *in vivo*. In this work, based on a recently developed linker-mediated vitrimer using metathesis reactions [33, 34], we propose a new reversible thermo-gelling

polymer. The polymer remains as an un-crosslinked liquid at low temperature and solidifies to a covalently crosslinked elastomer with increasing temperature. To describe the crosslinking of the designed thermo-gelling vitrimer, we formulate a mean field theory, which quantitatively agrees with coarse-grained computer simulations. Moreover, we find that the activation barrier of metathesis reactions plays a crucial role that it can drive the formation of an equilibrium gel with increasing temperature.

RESULTS

Model and mean field theory

We consider a system of volume V consisting of N_{poly} polymer chains, and each polymer chain comprises n connected hard spheres of diameter σ as the backbone, on which m precursors P are uniformly distributed. As shown in Fig. 1a, each P can react with a cross-linker molecule C or a protector molecule D to form a dangling PC or PD bond through metathesis reactions of reaction free energy $\Delta G_C = -\epsilon$ or $\Delta G_D = -\chi\epsilon$, respectively, with releasing a byproduct molecule B. Only dangling PC bonds can further react with another precursor P to form a P_2C crosslinking bond through the same metathesis reaction. To ensure no crosslinking formed at the low temperature limit, we consider $\chi > 1$. Small molecules B, C and D are modelled as hard spheres of diameter σ and controlled by the chemical potential μ_B , μ_C and μ_D , respectively. We assume that densities of small molecules in the reservoir remain constant for all temperature, i.e., $\beta\mu_B$, $\beta\mu_C$ and $\beta\mu_D$ do not change with T . Here $\beta = 1/k_B T$ with k_B and T the Boltzmann constant and temperature of the system, respectively. The packing fraction of polymer backbones is $\phi_p = \pi N_{poly} n \sigma^3 / 6$,

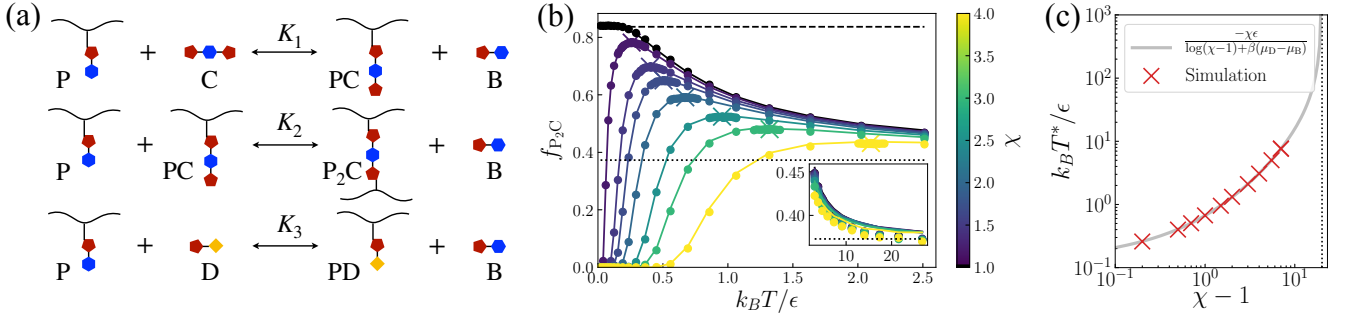


FIG. 1. **Entropy driven crosslinking vitrimers.** (a): Schematic representation of three metathesis reactions in the linker-mediated vitrimer protected by small protector molecule D. (b) The crosslinking degree f_{P_2C} as a function of temperature $k_B T/\epsilon$ for various χ from 1.0 to 4.0. Symbols are values obtained from simulations and solid lines are the theoretical prediction of Eq. 5 using K_2/K_1 calculated from simulations. The dashed and dotted horizontal lines are the values of f_{P_2C} at the low temperature limit with $\chi=1$, and at the high temperature limit theoretically predicted by Eq.5. \times symbols indicate the location of maximum value of f_{P_2C} obtained in simulations. Inset: f_{P_2C} as a function of $k_B T/\epsilon$ with at higher temperature showing the convergence to the theoretical prediction. (c) Optimal temperature $k_B T^*/\epsilon$ as a function of χ , where symbols are from simulations and the grey curve is the theoretical prediction of Eq. 10. The dotted vertical line shows the critical χ where T^* diverges. Here $N_{poly}=100$, $\phi_p=0.25$, $\chi_{att}=0$, $\beta\mu_B=-2$, $\beta\mu_C=-4$ and $\beta\mu_D=-5$.

and N_i is number of bonds or molecules in the system, where $i=P, PC, PD, P_2C, B, C$ and D . An infinitely deep square-well potential is employed to mimic the covalent bonds in the system,

$$V_{\text{bond}}(\mathbf{r}, \mathbf{r}') = \begin{cases} 0 & |\mathbf{r} - \mathbf{r}'| < r_{\text{bond}} \\ \infty & \text{else} \end{cases}, \quad (1)$$

where r_{bond} is the cut-off distance of the covalent bond. We use the square-well potential to model the van der Waals short range attraction between polymer backbones:

$$V_{\text{att}}(\mathbf{r}, \mathbf{r}') = \begin{cases} -\chi_{\text{att}}\epsilon & |\mathbf{r} - \mathbf{r}'| < r_{\text{att}} \\ 0 & \text{else} \end{cases}, \quad (2)$$

where χ_{att} and r_{att} are the strength and interaction range of the attraction, respectively. To be experimentally relevant, we choose $n=100$, $m=8$ and $r_{\text{bond}}=r_{\text{att}}=1.5\sigma$ throughout all simulations in this work.

The free energy of the system can be written as

$$\begin{aligned} \beta F = & \sum_{i=poly, B, C, D} N_i \left[\ln \left(\frac{N_i \Lambda^3}{V} \right) - 1 \right] \\ & + \sum_{i=P, PC, PD, P_2C} N_i \left[\ln \left(\frac{n_i \Lambda^3}{V_p} \right) - 1 \right] \\ & - N_{P_2C} k_B^{-1} \Delta S + \beta F_{\text{att}} + \beta F_{\text{HS}}^{\text{ex}} - \beta N_B \mu_B \\ & - \beta (N_{PC} + N_{P_2C} + N_C) \mu_C - \beta (N_{PD} + N_D) \mu_D \\ & + \beta (N_{PC} + 2N_{P_2C}) (\Delta G_C + \mu_B) + \beta N_{PD} (\Delta G_D + \mu_B), \end{aligned} \quad (3)$$

where Λ is the de Broglie wavelength. The first summation is on the ideal gas terms of polymer blobs (*poly*), byproduct molecules (B), free crosslinkers (C) and protectors (D). The second summation is on the ideal gas terms of precursors P, PC bonds, PD bonds and

P_2C bonds on a polymer confined within the volume V_p , which can be as the volume occupied by the polymer, and $n_i = N_i/N_{poly}$ is the number of bonds per polymer with $i=P, PC, PD, P_2C$. ΔS accounts for the entropy change of the system by forming a P_2C crosslinking bond, and F_{att} is the free energy contribution from the van der Waals short range attraction between polymer backbones. It is known that the structure of a homogeneous fluid is mainly determined by the repulsion between molecules [35]. Therefore, $F_{\text{att}} \approx -\chi_{\text{att}} \epsilon g(\phi)$, and $g(\phi)$ is a function of the total packing fraction of the system ϕ , which can be seen as the total number of non-bonded attractive pairs of backbone beads formed in the system. $F_{\text{HS}}^{\text{ex}}$ is the excess free energy accounting for the crowding effect, which we approximate with the Carnahan-Starling hard-sphere equation of state [36] (see Supplementary Materials S1), and it depends on the total packing fraction of the system ϕ . The other five terms arise from the bond swaps in metathesis reactions related with ΔG_C and ΔG_D , and the exchange of molecules with reservoir related with μ_B , μ_C and μ_D .

We define the crosslinking degree of the system as $f_{P_2C} = 2N_{P_2C}/(N_{poly}m)$ and the fraction of other bonds or molecules as $f_i = N_i/(N_{poly}m)$ with $i=P, PD, PC, B, C, D$, and

$$f_P + f_{PC} + f_{PD} + f_{P_2C} = 1. \quad (4)$$

With the saddle point approximation, i.e., $\partial F/\partial\{f_j\}=0$ with $j=PC, PD, P_2C$, we have $f_{PC} = f_P \Xi_{PC}$, $f_{PD} = f_P \Xi_{PD}$ and $f_{P_2C} = f_P^2 \Xi_{P_2C}$, where $\Xi_{P_2C} = (2m\Lambda^3/V_p) \exp[\beta(\mu_C - 2\mu_B + 2\epsilon + \mu_{\text{HS}}^{\text{ex}}) + k_B^{-1} \Delta S]$, $\Xi_{PC} = \exp[\beta(\mu_C - \mu_B + \epsilon)]$, and $\Xi_{PD} = \exp[\beta(\mu_D - \mu_B + \chi\epsilon)]$. $\mu_{\text{HS}}^{\text{ex}}$ is the excess free energy of hard spheres with packing fraction ϕ , which can be calculated by self-consistent iterations (see Supplementary Materials S1). Here we note that $\partial F_{\text{att}}/\partial f_j \approx -\chi_{\text{att}} \epsilon (\partial g/\partial \phi) (\partial \phi/\partial f_j) \approx 0$, with

the assumption that the system is mainly composed of polymer backbones, and the metathesis reactions have minor effects on the packing fraction of the system, i.e., $\partial\phi/\partial f_j \approx 0$. Substituting these terms into Eq. 4, we obtain

$$f_{P_2C} = \left(\sqrt{\Gamma^2 + 1} - \Gamma \right)^2, \quad (5)$$

with

$$\Gamma = \frac{1 + \Xi_{PC} + \Xi_{PD}}{2\sqrt{\Xi_{P_2C}}}. \quad (6)$$

Moreover, V_p and ΔS can be obtained by considering the chemical and reaction equilibrium (see Supplementary Materials S2), and

$$\frac{K_2}{K_1} = \frac{V}{N_{poly} V_p} e^{\Delta S/k_B}, \quad (7)$$

which can be measured in simulation or experiments.

Entropy driven crosslinking

First we investigate the crosslinking in the system without any short range van der Waals attraction, i.e., $\chi_{att} = 0$, and in Fig. 1b we plot the calculated f_{P_2C} from Monte Carlo (MC) simulations for various χ as functions of temperature $k_B T/\epsilon$ in comparison with the theoretical prediction of Eq. 5, in which the only input from simulations is K_2/K_1 . One can see that the results from computer simulation quantitatively agree with the mean field theory. At $\chi = 1$, f_{P_2C} reaches two different positive plateaus at $T \rightarrow 0$ and $T \rightarrow \infty$, respectively, with $f_{P_2C}(T \rightarrow 0) > f_{P_2C}(T \rightarrow \infty)$. When $\chi > 1$, as shown in Fig. 1b, $f_{P_2C}(T \rightarrow 0) \rightarrow 0$, and with increasing temperature, f_{P_2C} increases to reach a maximum at temperature T^* then decreases to approach the same plateau at high temperature, which does not depend on χ . These can be understood as follows. At the high temperature limit, $\beta\epsilon \rightarrow 0$, the crosslinking in the system is solely determined by entropy, and

$$\Gamma^\infty = \frac{1 + \Xi_{PC}^\infty + \Xi_{PD}^\infty}{2\sqrt{\Xi_{P_2C}^\infty}}, \quad (8)$$

with $\Xi_{PC}^\infty = \exp[\beta(\mu_C - \mu_B)]$, $\Xi_{PD}^\infty = \exp[\beta(\mu_D - \mu_B)]$, and $\Xi_{P_2C}^\infty = (2m\Lambda^3/V_p) \exp[\beta(\mu_C - 2\mu_B + \mu_{HS}^{ex}) + k_B^{-1}\Delta S]$, which does not depend on χ . This can be further used to calculate $f_{P_2C}^\infty$ using Eq. 5. Moreover, at the low temperature limit, i.e., $\beta\epsilon \rightarrow \infty$, when $\chi = 1$, the saddle-point solution of Γ can be obtained by the Lagrange multiplier method (see Supplementary Materials S4):

$$\Gamma^0 = \frac{\Xi_{PC}^\infty + \Xi_{PD}^\infty}{2\sqrt{\Xi_{P_2C}^\infty}}, \quad (9)$$

with which we can calculate the low temperature plateau $f_{P_2C}^0$ for $\chi = 1$ with Eq. 5. One can see that $\Gamma^\infty > \Gamma^0$, which implies $f_{P_2C}^\infty < f_{P_2C}^0$, as Eq. 5 is a monotonically decreasing function of Γ . When $\chi > 1$, as the formation of PD bonds is more energetically favourable than that of PC bonds, the crosslinking is prevented at the low temperature limit, and at small χ , the competition between entropy driven crosslinking and enthalpy driven protection by PD bonds leads to the non-monotonic behaviour of f_{P_2C} with increasing T . The optimal temperature T^* , where f_{P_2C} reaches the maximum can be obtained by solving $\partial f_{P_2C}/\partial\beta = 0$ equivalent to $\partial\Gamma/\partial\beta = 0$, which is

$$k_B T^* = \frac{-\chi\epsilon}{\log(\chi - 1) + \beta(\mu_D - \mu_B)}. \quad (10)$$

T^* is a positive number when $1 < \chi < 1 + \exp[\beta(\mu_B - \mu_D)]$. When $\chi > 1 + \exp[\beta(\mu_B - \mu_D)]$, the protecting effect of PD bonds is too strong, and f_{P_2C} increases monotonically with increasing temperature. As shown in Fig. 1c, the theoretically predicted T^* agrees quantitatively with computer simulations. Intriguingly, Eq. 10 does not need any input from simulation or experiments, and one can also see that the optimal temperature T^* does not depend on the backbone packing fraction ϕ_p or the crosslinker chemical potential $\beta\mu_C$, which is confirmed in our MC simulations (Fig. S1ac). However, the height of f_{P_2C} peak does depend on $\beta\mu_C$, and it changes non-monotonically (Fig. S1c). This non-monotonic dependence originates from an entropic effect recently found in linker-mediated vitrimers [34, 37, 38]. Moreover, the position and height of f_{P_2C} can be also tuned by changing the concentration of B and D molecules, i.e., $\beta\mu_B$ and $\beta\mu_D$ (Fig. S1bd).

Effects of short range attraction between polymers

As in realistic vitrimers, there are always some short range van der Waals attraction between polymer backbones driving the gelation at low temperature, we investigate the system with weak attraction. In Fig. 2a, we plot f_{P_2C} as a function of $k_B T/\epsilon$ for systems at $\chi_{att} = 0.1$ of various polymer packing fraction $\phi_p = 0.1$ to 0.3 and $\chi = 2$. One can see that similar to the system without attraction, with increasing temperature, f_{P_2C} first increase and then decrease to approach a plateau at high temperature, and the results from computer simulation agree quantitatively with the theoretical prediction (Eq. 5). We further simulate the vitrimer system with changing χ_{att} at $\phi_p = 0.2$ and $\chi = 2$, and the results are shown in Fig. 2b. At high temperature, the simulation results agree very well with theoretical prediction, while below certain temperature T_c , the discrepancy appears. To understand the cause for the discrepancy, we plot the corresponding pressure $P\sigma^2/\epsilon$ as a function of temperature in the upper

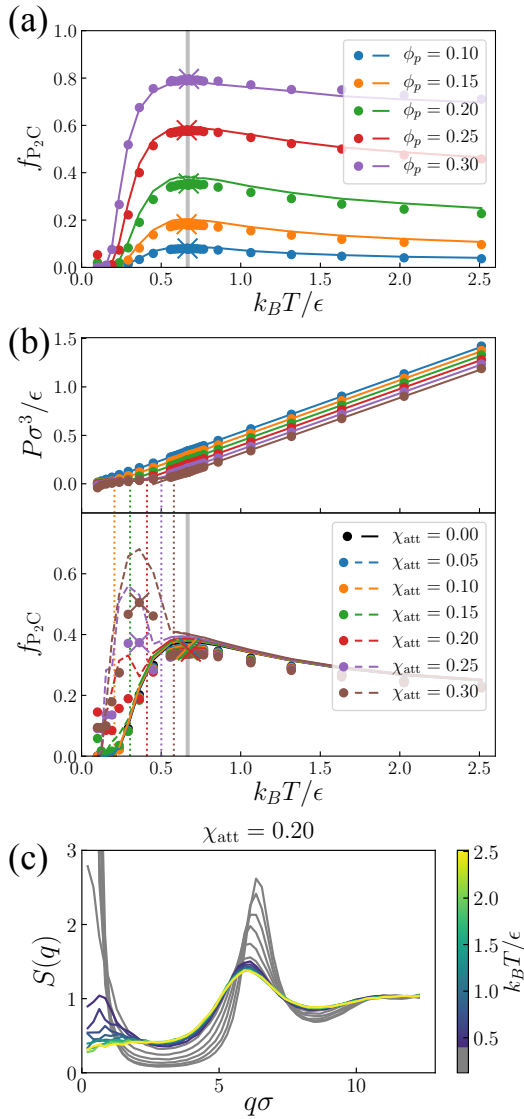


FIG. 2. **Effects of short range attraction.** (a): f_{P_2C} as a function of temperature $k_B T / \epsilon$ for various ϕ_p at $\chi_{att} = 0.1$. (b): f_{P_2C} (lower panel) and pressure $P\sigma^3/\epsilon$ (upper panel) as a function of temperature $k_B T / \epsilon$ for different short range attraction χ_{att} . Upper panel: the symbols are from simulations and the lines are linear fits in the two different phases, and the position of turning-points, critical temperatures T_c , are indicated by dotted vertical lines. Lower panel: dashed and solid curves are the theoretical prediction of Eq. 5 above and below the critical temperature T_c , respectively, with the measured K_2/K_1 from simulations. (c) Structure factor $S(q)$ for systems at different temperatures, where the curves below T_c are grey. Here $N_{poly} = 100$, $\phi_p = 0.20$, $\chi = 2.0$, $\beta\mu_B = -2$, $\beta\mu_C = -4$ and $\beta\mu_D = -5$.

panel of Fig. 2b. We see that with decreasing temperature, the slope of $P-T$ curve has a turning point coinciding with the temperature threshold T_c (as indicated by the dotted vertical lines), below which the difference between simulation and theory appears. As the slope change in $P-T$ curve normally suggests a phase separation, we plot the structure factor of the system with

χ_{att} at various temperature in Fig 2c. One can see that below T_c , $S(q)$ diverges at small q , which is a signature of phase separation. This suggests that the discrepancy between the theoretical prediction and computer simulations at low temperature is due to the attraction induced phase separation, which creates interfaces in the system. Although in the thermodynamic limit, the interfacial free energy is negligible, in practice, polymer systems can hardly reach a fully phase separated equilibrium state, and this makes the free energy in Eq. 3 not able to correctly model the system.

Thermo-gelling vitrimers

Next, we perform molecular dynamics (MD) simulations to investigate the thermo-induced gelation of vitrimers. We assume all metathesis reactions sharing the same activation barrier ΔG_b , and the rate of reaction $k = \nu_0 \exp(-\beta[\Delta G_b + \max(\Delta G, 0)])$ with ΔG the reaction free energy. $\nu_0 = 1/\tau_{MD}$ is the kinetic prefactor, and $\tau_{MD} = \sqrt{m_b \sigma^2 / \epsilon}$ is the time unit of MD simulations with m_b the mass of a polymer bead, where we assume all the small molecules, i.e., B, C and D, having the same mass as a polymer bead. The activation barrier ΔG_b does not change any thermodynamic property of the system, while it does control the dynamic properties [39]. We perform hybrid event-driven molecular dynamics - Monte Carlo (EDMD-MC) NVT simulations for a system with $\phi_p = 0.2$, $\chi = 2.0$ and $\chi_{att} = 0.1$ at different temperatures starting from equilibrated configurations from grand canonical MC simulations. We plot the structural relaxation time τ_α as a function of temperature in comparison with the corresponding f_{P_2C} in Fig. 3a, which is defined as $F_s(q, \tau_\alpha) = e^{-1}$ with $F_s(\cdot)$ the intermediate scattering function. As here the diffusion is mainly through the reptation of polymer chains, we choose $q = 2\pi / (n\sigma)$. One can see that when $\Delta G_b = 0$, τ_α decreases monotonically with increasing temperature, despite the increased crosslinking degree f_{P_2C} . This is because that increasing temperature increases the mobility of molecules in the system, and due to the zero activation barrier of metathesis reaction, the crosslinking has minimal effects on the dynamics of the system. This is similar to the first generation vitrimer, which is a liquid at high temperature although fully crosslinked [40]. With increasing ΔG_b , the effect of crosslinking on the dynamics of the system becomes more pronounced, and τ_α starts to increase with temperature at about $0.3\epsilon/k_B$ to develop a peak, where f_{P_2C} starts to increase as shown in Fig. 3a. When $\Delta G_b = 10\epsilon$, τ_α diverges between $k_B T / \epsilon = 0.5$ and 1.0 , and the corresponding $F_s(q, t)$ are shown in Fig. 3b, which develops a plateau at both $k_B T / \epsilon \leq 0.1$ and $0.5 < k_B T / \epsilon < 1$. This implies that the system becomes a gel at both low and high temperatures. To distinguish the property of gels formed at different

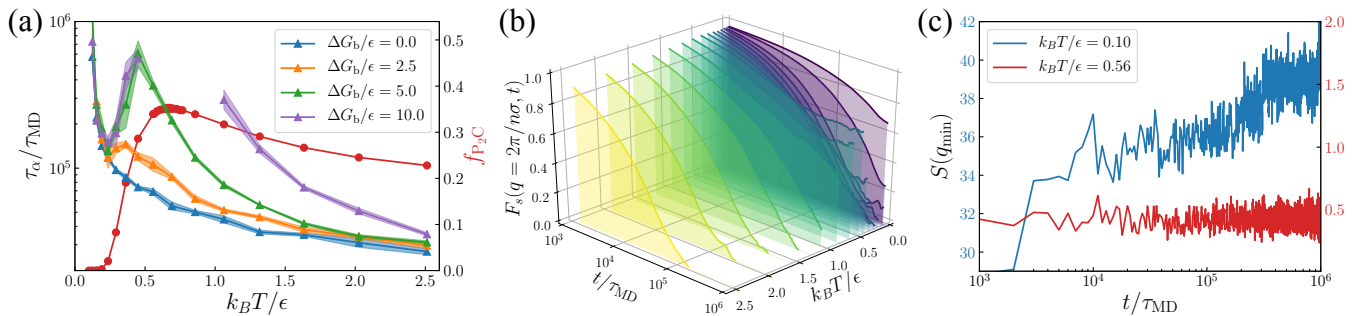


FIG. 3. **Thermo-gelling vitrimers.** (a): The structural relaxation time τ_α (left) and crosslinking degree f_{P_2C} (right) as a function temperature $k_B T/\epsilon$ for various activation barrier ΔG_b . We note that f_{P_2C} does not depend on ΔG_b . (b): The intermediate scattering function $F_s(q, t)$ with $q=2\pi/n\sigma$ at various temperature $k_B T/\epsilon$ with $\Delta G_b/\epsilon=10.0$. (c): Structure factor $S(q_{\min})$ with $q_{\min}=2\pi/V^{1/3}$ as a function of t at different temperatures. Here $\phi_p=0.20$, $\chi=2.0$ and $\chi_{\text{att}}=0.1$ with N_B , N_C and N_D obtained from MC simulations with $\beta\mu_B=-2$, $\beta\mu_C=-4$ and $\beta\mu_D=-5$.

temperatures, we plot the time evolution of $S(q_{\min})$ in Fig. 3c, which shows the large-scale structural change in the system. One can see that at the low temperature, i.e., $k_B T/\epsilon=0.1$, $S(q_{\min})$ increases significantly with time suggesting the system undergoing a kinetically arrested phase separation, which is a typical signature of gelation induced by short range attraction [41]. However, as shown in Fig. 3c, in a high temperature gel, i.e., $k_B T/\epsilon=0.56$, $S(q_{\min})$ does not change with time, which suggests that there is no structural change in the system, and the thermo-gelling vitrimer is an equilibrium gel not subject to any thermodynamic instability [42, 43].

DISCUSSION AND CONCLUSION

In conclusion, we have proposed a novel thermo-gelling vitrimer, in which at low temperature, the crosslinking is prevented by the protector, i.e., D molecules, and with increasing temperature, the entropy driven crosslinking occurs, which drives the gelation of the system. We formulate a mean field theory to describe the crosslinking, which agrees quantitatively with coarse grained computer simulations above the gas-liquid phase separation temperature induced by the short range van der Waals attraction in the system. Further molecular dynamics simulations show that the activation barrier of the metathesis reaction plays a crucial role during the thermo-gelling process, and it can be controlled by using different catalysts experimentally. Moreover, we show that the resulting thermo-induced gelation is an equilibrium gel not subject to any thermodynamic instability. Similar thermo-gelling systems were studied previously in patchy colloidal systems [44] and DNA nano stars [14]. The difference is that the designed vitrimers here are covalently crosslinked, which is essentially a thermo-crosslinking elastomer. Because of the nature of metathesis reactions in vitrimers, the activation barrier can be tuned using catalysts to realize the equilibrium gel with increas-

ing temperature, and this is qualitatively different from conventional gelations induced by short ranged attraction, which are essentially kinetically arrested phase separations [41]. Moreover, at high temperature, different from the thermo-gelling systems using weak interactions, e.g., hydrogen bonds, our designed vitrimers are always crosslinked because of entropy, and mechanical properties can be tuned reversibly *in situ* by changing the activation barrier using catalysts and/or adjusting the concentration of B and D molecules. The concept of vitrimers is a versatile tool that is applicable to nearly all types of polymers. Therefore, by adopting an appropriate polymer system, the thermo-gelling vitrimer designed here should be promising for biomedical applications. For example, based on the designed scheme, one could employ biocompatible silyl ether metathesis to fabricate thermo-responsive biomaterials for tissue repair and injectable implants in non-invasive surgeries [28, 45].

METHODS

Monte Carlo Simulations. We perform MC simulations to investigate the equilibrium properties of the thermo-crosslinking vitrimer. Assuming the bulk density conservation of B, C and D when temperature varies, we adopt grand canonical $\beta\mu_B\mu_C\mu_D-N_{\text{poly}}VT$ MC simulations to simulate the coarse-grained hard-sphere-chain system, with the temperature unit ϵ/k_B . Simulations are performed with N_{poly} polymer chains with n beads per chain, where periodic boundary conditions are applied in all three dimensions with the cubic box volume $V=N_{\text{poly}}n/\phi_p$. The translational moves of particles are implemented by the straight event-chain algorithm [46, 47], in which the length of each event is fixed at $L_c=10\sigma$, and the pressure P of the system can be

calculated by the mean excess chain displacement

$$P = k_B T \rho \left\langle \frac{x_{\text{final}} - x_{\text{initial}}}{L_c} \right\rangle_{\text{chains}}, \quad (11)$$

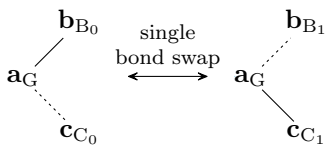
where x_{initial} and x_{final} are the projection of initial and final particle positions on the chain direction of each event chain, ρ is number density of the particles and $\langle \cdot \rangle_{\text{chains}}$ calculates the average over all event chains. Molecules B, C and D are inserted or removed using the conventional grand canonical MC method. Besides, we devise a simple bond swap algorithm to simulate reversible bond swap metathesis reactions in the vitrimer system (see below), respecting the detailed balance. The ratio of three types of trial moves, translational moves, inserting/removing molecules and bond swaps, is 1:4:5. In each simulation, we perform 10^9 MC moves for equilibration and 10^9 MC moves for sampling.

Hybrid EDMD–MC simulations. We perform the hybrid EDMD–MC simulation [39, 48, 49] to measure the intermediate scattering function $F_s(q, t)$ and the structural relaxation time τ_α in the canonical (NVT) ensemble starting from equilibrated configurations from our grand canonical MC simulations with Anderson thermostat [50, 51]. All the bond swaps in metathesis reactions are done by the MC algorithm below [50]. In our simulations, $N_{\text{poly}} m$ bond swap attempts are tried per time interval τ_{MD} . Each simulation consists of $10^6 \tau_{\text{MD}}$ for equilibration and $10^6 \tau_{\text{MD}}$ for sampling. The self-intermediate scattering function $F_s(q, t)$ is a common indicator for structural relaxation in MD simulations [39]:

$$F_s(q, t) = \frac{1}{n N_{\text{poly}}} \left\langle \sum_{j=1}^{n N_{\text{poly}}} \exp[i\mathbf{q} \cdot (\mathbf{r}_j(t) - \mathbf{r}_j(0))] \right\rangle, \quad (12)$$

which calculates over all backbone beads on the vitrimers.

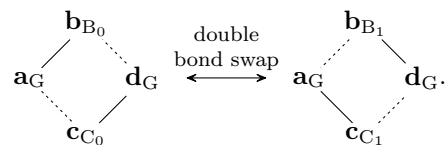
Bond swap algorithm. In our MC simulations, a typical reversible single bond-swap reaction is



where $\mathbf{a}/\mathbf{b}/\mathbf{c}$ and $G/A_0/A_1/B_0/B_1$ are the specific particles/beads as shown in the three kinds of reactions in Fig. 1a. The proposed move for the forward reaction can be constructed by the following two steps:

1. Choose a *pivot* particle \mathbf{a} (type G) bounded with \mathbf{b} (type $B_0 = \text{P, PC, P}_2\text{C}$ or PD) with probability $p(\mathbf{a})$ (there is precisely one bond can be swapped for each pivot particle);
2. Choose a neighboring potentially reactive particle \mathbf{c} (type $C_0 = \text{B, C, D}$ or PC) within the distance r_{bond} randomly with probability $h(\mathbf{c}_{C_0}|\mathbf{a})$;

One can see the above bond swap move does not change the number of neighbor potentially reactive particles and bonds of \mathbf{a} , hence both before and after a bond swap move, $h(\mathbf{c}_{C_0}|\mathbf{a}) = h(\mathbf{b}_{B_1}|\mathbf{a})$. For the first and third reaction in Fig. 1a, the acceptance probability of the proposed move of forward and backward reactions are $\exp(-\beta\Delta G)$ and $\exp(\beta\Delta G)$, respectively, with the free energy of the forward reaction ΔG . For the second reaction in Fig. 1a, we double the forward reaction flux to equalize the flux between the two states before and after the reaction [34]. Furthermore, for mimicking the actual topology and reaction dynamics of vitrimers, i.e., the covalent bond-exchange dynamics in Fig. S3, we perform additional double bond swap reactions in the EDMD–MC simulation as follows, before and after which no chemical potential change in the system:



We randomly choose each specific bond swap move in three steps:

1. Select a *pivot* particle \mathbf{a} (type G) bounded with \mathbf{b} (type $B_0 = \text{P, PC, P}_2\text{C}$ or PD) with probability $p(\mathbf{a})$;
2. Select a neighboring potentially reactive particle \mathbf{c} other than \mathbf{b} (type $C_0 = \text{B, C, D, PB, PC, P}_2\text{C}$ or PD) within randomly the distance r_{bond} with probability $h(\mathbf{c}_{C_0}|\mathbf{a})$.
3. Select a reaction type (single-bond/double-bond) with probability $g(\mathbf{c}_{C_0}|\mathbf{b}_{B_0})$.

Similarly, here $h(\mathbf{c}_{C_0}|\mathbf{a}) = h(\mathbf{b}_{B_1}|\mathbf{a})$. g accounts for the the number of possible bonds combinations, and if $\mathbf{b}_{B_0}/\mathbf{c}_{C_0}$ can undergo both single-bond swap and double-bond swap, $g(\mathbf{c}_{C_0}|\mathbf{b}_{B_0}) = 0.5$, otherwise, $g(\mathbf{c}_{C_0}|\mathbf{b}_{B_0}) = 1$. Additionally, we consider that all metathesis reactions share the same activation barrier ΔG_b and activation free energy is $\Delta G_b + \max(\Delta G, 0)$. A bond swap attempt first needs to overcome the energy barrier with probability $\text{acc}_b = \exp(-\Delta G_b/k_B T)$, and then is accepted with the probability

$$\text{acc}_r = \min \left[1, \frac{g(\mathbf{b}_{b_0}|\mathbf{a}_{a_0})}{g(\mathbf{a}_{a_1}|\mathbf{b}_{b_1})} \exp(-\beta\Delta G) \right], \quad (13)$$

where ΔG is the bond swap reaction free energy.

SUPPLEMENTARY MATERIALS

Supplementary material for this article is available at XXXXX-XXXXX

Section S1. Mean field theory for thermo-crosslinking vitrimers.

Section S2. Chemical equilibrium and reaction equilibrium.

Section S3. Mean field theory at the high temperature limit.

Section S4. Mean field theory at the low temperature limit.

Acknowledgments: We thank Dr. Shilong Wu and Prof. Quan Chen in Chinese Academy of Sciences for fruitful discussions. **Funding:** This work is supported by the Academic Research Fund from Singapore Ministry of Education Tier 1 Grant (RG59/21) and Tier 2 Grant (MOE2019-T2-2-010). **Author contributions:** R.N. conceived the research; X.X. formulated the mean field theory and performed the Monte Carlo simulations; P. R. performed the molecular dynamics simulations; all authors discussed the results and wrote the manuscript. **Competing interests:** The authors declare that they have no competing interests. **Data and materials availability:** All data needed to evaluate the conclusions in the paper are presented in the paper and/or the Supplementary Materials. Additional data related to this paper may be requested from the authors.

* These authors contributed equally.

† r.ni@ntu.edu.sg

- [1] D. Roy, W. L. A. Brooks, and B. S. Sumerlin, *Chem. Soc. Rev.* **42**, 7214 (2013).
- [2] C. d. I. H. Alarcón, S. Pennadam, and C. Alexander, *Chem. Soc. Rev.* **34**, 276 (2005).
- [3] S. Qiao and H. Wang, *Nano Res.* **11**, 5400 (2018).
- [4] Q. Q. Dou, S. S. Liow, E. Ye, R. Lakshminarayanan, and X. J. Loh, *Adv. Healthcare Mater.* **3**, 977 (2014).
- [5] A. Lendlein and R. Langer, *Science* **296**, 1673 (2002).
- [6] A. K. Bajpai, S. K. Shukla, S. Bhanu, and S. Kankane, *Prog. Polym. Sci.* **33**, 1088 (2008).
- [7] N. Nath and A. Chilkoti, *Adv. Mater.* **14**, 1243 (2002).
- [8] W. Chen, L. Qu, D. Chang, L. Dai, S. Ganguli, and A. Roy, *Chem. Commun.*, 163 (2008).
- [9] X. Laloyaux, E. Fautré, T. Blin, V. Purohit, J. Leprince, T. Jouenne, A. M. Jonas, and K. Glinel, *Adv. Mater.* **22**, 5024 (2010).
- [10] A. S. Hoffman and P. S. Stayton, *Prog. Polym. Sci.* **32**, 922 (2007).
- [11] N. Shamim, L. Hong, K. Hidajat, and M. S. Uddin, *Sep. Purif. Technol.* **53**, 164 (2007).
- [12] S. Fujishige, K. Kubota, and I. Ando, *J. Phys. Chem.* **93**, 3311 (1989).
- [13] M. B. Huglin and M. A. Radwan, *Polym. Int.* **26**, 97 (1991).
- [14] F. Bomboi, F. Romano, M. Leo, J. Fernandez-Castanon, R. Cerbino, T. Bellini, F. Bordi, P. Filetici, and F. Sciortino, *Nat. Commun.* **7**, 1 (2016).
- [15] M. Kapnistos, D. Vlassopoulos, G. Fytas, K. Mortensen, G. Fleischer, and J. Roovers, *Phys. Rev. Lett.* **85**, 4072 (2000).
- [16] H. Zhang, L. Yu, and J. Ding, *Macromolecules* **41**, 6493 (2008).
- [17] H. J. Moon, D. Y. Ko, M. H. Park, M. K. Joo, and B. Jeong, *Chem. Soc. Rev.* **41**, 4860 (2012).
- [18] M. Yuan, B. Bi, J. Huang, R. Zhuo, and X. Jiang, *Carbohydr. Polym.* **192**, 10 (2018).
- [19] Y. Dong, W. Hassan, Y. Zheng, A. O. Saeed, H. Cao, H. Tai, A. Pandit, and W. Wang, *J. Mater. Sci. Mater. Med.* **23**, 25 (2012).
- [20] P. van de Wetering, A. T. Metters, R. G. Schoenmakers, and J. A. Hubbell, *J. Controlled Release* **102**, 619 (2005).
- [21] S. Sakai, K. Hirose, K. Moriyama, and K. Kawakami, *Acta Biomater.* **6**, 1446 (2010).
- [22] F. Lee, J. E. Chung, and M. Kurisawa, *J. Controlled Release* **134**, 186 (2009).
- [23] T. Vermonden, N. E. Fedorovich, D. van Geemen, J. Alblas, C. F. van Nostrum, W. J. A. Dhert, and W. E. Hennink, *Biomacromolecules* **9**, 919 (2008).
- [24] S. H. Lee, Y. Lee, S. W. Lee, H.-Y. Ji, J.-H. Lee, D. S. Lee, and T. G. Park, *Acta Biomater.* **7**, 1468 (2011).
- [25] P. Nezhad-Mokhtari, M. Ghorbani, L. Roshangar, and J. S. Rad, *Int. J. Biol. Macromol.* **139**, 760 (2019).
- [26] F. Cellesi, N. Tirelli, and J. A. Hubbell, *Macromol. Chem. Phys.* **203**, 1466 (2002).
- [27] D. Montarnal, M. Capelot, F. Tournilhac, and L. Leibler, *Science* **334**, 965 (2011).
- [28] C. A. Tretbar, J. A. Neal, and Z. Guan, *J. Am. Chem. Soc.* **141**, 16595 (2019).
- [29] D.-C. Wu, X. J. Loh, Y.-L. Wu, C. L. Lay, and Y. Liu, *J. Am. Chem. Soc.* **132**, 15140 (2010).
- [30] M. Pepels, I. Pilot, B. Klumperman, and H. Goossens, *Polym. Chem.* **4**, 4955 (2013).
- [31] I. S. Cho and T. Ooya, *J. Biomater. Sci. Polym. Ed.* **29**, 145 (2018).
- [32] L. Jiang, Y. Tian, J. Cheng, and J. Zhang, *Polym. Chem.* **12**, 6527 (2021).
- [33] M. Röttger, T. Domenech, R. v. d. Weegen, A. Breuillac, R. Nicolaÿ, and L. Leibler, *Science* **356**, 62 (2017).
- [34] Q. L. Lei, X. Xia, J. Yang, M. P. Ciamarra, and R. Ni, *Proc. Natl. Acad. Sci. U. S. A.* **117**, 27111 (2020).
- [35] J. D. Weeks, D. Chandler, and H. C. Andersen, *J. Chem. Phys.* **54**, 5237 (1971).
- [36] J.-P. Hansen and I. R. McDonald, *Theory of simple liquids* (Elsevier, 1990).
- [37] S. Wu, H. Yang, S. Huang, and Q. Chen, *Macromolecules* **53**, 1180 (2020).
- [38] X. Xia, H. Hu, M. P. Ciamarra, and R. Ni, *Sci. Adv.* **6**, eaaz6921 (2020).
- [39] J.-B. Wu, S.-J. Li, H. Liu, H.-J. Qian, and Z.-Y. Lu, *Phys. Chem. Chem. Phys.* **21**, 13258 (2019).
- [40] D. Montarnal, M. Capelot, F. Tournilhac, and L. Leibler, *Science* **334**, 965 (2011).
- [41] P. J. Lu, E. Zaccarelli, F. Ciulla, A. B. Schofield, F. Sciortino, and D. A. Weitz, *Nature* **453**, 499 (2008).
- [42] F. Sciortino and E. Zaccarelli, *Curr. Opin. Colloid Interface Sci.* **30**, 90 (2017).
- [43] P. I. Hurtado, L. Berthier, and W. Kob, *Phys. Rev. Lett.* **98**, 135503 (2007).
- [44] S. Roldán-Vargas, F. Smallenburg, W. Kob, and F. Sciortino, *Sci. Rep.* **3**, 1 (2013).
- [45] M. C. Parrott, J. C. Luft, J. D. Byrne, J. H. Fain, M. E. Napier, and J. M. DeSimone, *J. Am. Chem. Soc.* **132**, 17928 (2010).

- [46] E. P. Bernard, W. Krauth, and D. B. Wilson, *Phys. Rev. E* **80**, 056704 (2009).
- [47] T. A. Kampmann, H.-H. Boltz, and J. Kierfeld, *J. Chem. Phys.* **143**, 044105 (2015).
- [48] E. B. Stukalin, L.-H. Cai, N. A. Kumar, L. Leibler, and M. Rubinstein, *Macromolecules* **46**, 7525 (2013).
- [49] R. S. Hoy and G. H. Fredrickson, *J. Chem. Phys.* **131**, 224902 (2009).
- [50] D. Frenkel and B. Smit, *Understanding molecular simulation: from algorithms to applications*, Vol. 1 (Elsevier, 2001).
- [51] H. C. Andersen, *J. Chem. Phys.* **72**, 2384 (1980).